International Journal of Innovative Technology and Exploring Engineering (IJITEE)
ISSN: 2278-3075 (Online), Volume-14 Issue-10, September 2025

Magnetoresistance and Carrier Collection in Bifacial Multicrystalline-Si Solar Cells: Role of Base Thickness and Illumination Mode

Moussa Toure, Mamadou Lamine Samb, Youssou Gning, Aly Toure, Ahmed Mohamed-Yahya

***Abstract*: *We investigate how weak transverse magnetic fields ($B = 10^{-4}$ to 10^{-3} T) influence bifacial multicrystalline-silicon photovoltaic cells operated near open-circuit conditions, focusing on the photovoltage (V_{ph}), photocurrent density (J_{ph}), and the apparent series resistance (Rs) as functions of base thickness (e = 100–400 µm) and illumination mode (front, rear, dual). J_{ph}–V_{ph} characteristics reveal a systematic increase of Rs with B, whose magnitude depends strongly on e and illumination: the effect is maximal under rear illumination, mitigated under dual illumination, and moderate under front illumination. Under rear illumination, increasing e markedly reduces carrier collection; for illustration, J_{ph} and V_{ph} drop from ≈10 mA·cm^{-2} and 0.34 V to ≈0 mA·cm^{-2} and 0.23 V when e increases from 100 to 400 µm. To quantify this behavior, we analyze $R_s(e, B)$ and the absolute change ΔR_s (maximized over the tested field window). Because the carrier-collection velocity (CCV) can vary with operating conditions, we report extractions in which CCV is either freely fitted or held fixed at 60.256 cm·s^{-1} to isolate the magnetic contribution to R_s. The interpretation follows a magnetoresistive framework: the Lorentz force reduces the effective mobility µ(B) and, via the Einstein relation, the diffusion coefficient D(B). In the Drude limit for $B \perp J$, the longitudinal diffusion follows $D^*(B)=D/[1+(\mu B)^2]$, implying a shortened diffusion length and reduced conductance. At millitesla fields, however, the intrinsic reduction of D is slight; the dominant contributions to the "apparent" Rs arise from surfaces and contacts (passivation quality, metallization), current-spreading in the base, extraction geometry (sheet vs. bulk paths), and injection level. A joint parametric extraction of {J_0, n, R^s, R_{sh}} by illumination mode and thickness is essential to explain high-voltage slopes and to link transport parameters to performance. These findings identify practical levers, thickness selection, improved surface passivation, optimized contact design, and illumination strategy, to mitigate magnetically induced increases in R_s. They also motivate future work on field orientation, temperature dependence, and spatial mapping of R_s to localize resistive bottlenecks and guide device engineering.*

Keywords*: *Magnetoresistance; Bifacial Solar Cells; Multicrystalline Silicon; Carrier Collection; Series Resistance; Base Thickness

Abbreviations:
3D: Three-Dimensional
AM1.5: Air Mass 1.5
B: Magnetic Flux Density
BSF: Back Surface Field
CCV: Carrier-Collection Velocity
D: Diffusion Coefficient at B = 0
D*(B): Effective Diffusion Coefficient Under Magnetic Field
mc-Si: Multicrystalline Silicon
PV: Photovoltaic
R_{sh}: Shunt Resistance
R_s: Series Resistance
SCR: Space-Charge Region
SRV: Surface Recombination Velocity
T: Absolute Temperature
V_{oc}: Open-Circuit Voltage
V_{ph}: Photovoltage

I. INTRODUCTION

This work investigates bifacial multicrystalline-silicon solar cells under modest external magnetic fields $B = 1e-4$ to $1e-3$ T, examining how photovoltage, photocurrent density, and series resistance R_s depend on base thickness ($e = 100 - 400$ µm) and illumination mode (front, rear, dual) in the near-open-circuit regime. We present $J_{ph} - V_{ph}$ curves together with $R_s(e, B)$ and its absolute change ΔR_s, highlighting strong sensitivity under rear illumination and mitigation under dual illumination, in line with bifacial operation and thickness-dependent transport [1]. Across most measurements, the carrier-collection velocity (CCV) is varied; only where explicitly indicated do we include a reference panel with CCV fixed at $60.256\, cm.s^{-1}$ to compare the absolute change in series resistance. Interpretation follows a magnetoresistive framework, characterised by reduced mobility and diffusion under B, and elongated spreading paths, coupled with recombination and passivation, as well as surface and contact considerations. Reported magnetic-field effects on PV behavior and mc-Si devices provide context for the observed trends, while base-thickness optimization under field and 3D/bifacial modelling inform design choices in thickness, passivation, and contact engineering [2].

Manuscript received on 28 August 2025 | Revised Manuscript received on 06 September 2025 | Manuscript Accepted on 15 September 2025 | Manuscript published on 30 September 2025.
*Correspondence Author(s)
Moussa TOURE*, Professor, Department of Physics and Chemistry, University Iba Der Thiam of Thies, Thies, Senegal, Email ID: moussa.toure@univ-thies.sn, ORCID ID: 0009-0005-4663-9533
Mamadou Lamine Samb, Associate Professor, Department of Physics and Chemistry, University of Iba Der Thiam of Thies, Thies, Senegal, Email ID: mlsamb@univ-thies.sn, ORCID ID: 0000-0003-0695-553X
Dr. Youssou N Ging, Professor, Department of Physics and Chemistry, University Iba Der Thiam of Thies, Thies, Senegal, Email ID: youssou.gning@univ-thies.sn, ORCID ID: 0000-0003-2486-6944
Aly Toure, Student, Department of Physique Chimie, University Iba Der Thiam of Thies, Thies, Senegal. Email ID: aly.toure1@univ-thies.sn, ORCID ID: 0009-0009-9736-7733
Ahmed Mohamed-Yahya, Associate Professor, Department of Physics, Université de Nouakchott Al Aasriya, Nouakchott, Mauritania. Email ID: biyah2001@yahoo.fr, ORCID ID: 0000-0002-3596-1819

II. PHYSICAL MODEL AND MAGNETIC PARAMETERS

A. Description of the Simulation Solar Cell

The study is based on a three-dimensional columnar model centred on a single grain of polycrystalline silicon. A magnetic field is applied perpendicularly to the plane of the junction, thereby altering the charge carrier transport conditions. In this context, the expressions for the diffusion coefficient D*(B) and the diffusion length L*(B) are given respectively by:

$$D^*(B) = D/(1+(\mu B)^2) \quad \dots \quad (1)$$

$$L^*(B) = \sqrt{D^*.\tau} \quad \dots \quad (2)$$

where:

1). D: classical diffusion coefficient in the absence of a magnetic field ($cm^2 \cdot s^{-1}$),
2). μ : charge carrier mobility ($cm^2 \cdot V^{-1} \cdot s^{-1}$)
3). B: applied magnetic field intensity (T),
4). τ : average lifespan of minority shareholders (s),

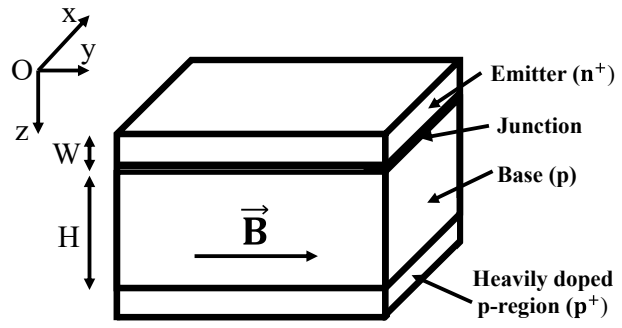

[Fig.1: Simulated Solar Cell Model]

As illustrated in the previous figures, the bifacial solar cell under investigation comprises four central functional regions:

1). The emitter, of n^+ type and reduced thickness (ranging from 0.5 to 1 μm),
2). The p–n junction, also referred to as the space charge region (SCR),
3). The base, of p-type,
4). The Back Surface Field (BSF) region.

To streamline the model, the emitter contribution to photocurrent generation is neglected relative to that of the base, and any internal crystalline electric field within the base is ignored; only the depletion-region field across the junction is retained. A three-dimensional framework is adopted with the intersection located at the origin of the z-axis; the junction plane defines the origin of the (x, y) coordinates. The base thickness, H, is treated as a variable parameter in the range of 100–400 μm. Under steady illumination, the minority-carrier continuity equation in the base takes the form:

$$\frac{\partial^2}{\partial x^2}\delta(x,y,z) + [1+(\mu B)^2]\frac{\partial^2}{\partial y^2}\delta(x,y,z) + \frac{\partial^2}{\partial z^2}\delta(x,y,z) - \frac{\delta(x,y,z)}{L^{*2}} = -\frac{G(z)}{D^*} \quad \dots \quad (3)$$

where D* represents the diffusion coefficient and L* represents the diffusion length.

G(z) represents the generation rate, and its expression is given by the following equation (4):

$$G(z) = n\sum_{i=1}^{3} a_i e^{(-b_i z)} \quad \dots \quad (4)$$

a_i and b_i are coefficients derived from the modelling of the generation rate, considering the entire solar radiation spectrum when n is equal to 1.5 AM;

Where n is the number of suns.

The general solution of this continuity equation is given by the following expression (5):

$$\delta(x,y,z) = \sum_j \sum_k Z_{j.k}(z)\cos C_j \times \cos C_k(B)y \quad \dots \quad (5)$$

with :

$$C_k(B) = \frac{C_k}{C(B)} \quad \dots \quad (6)$$

By imposing the boundary conditions at the grain boundaries, the coefficients C_k and C_j are obtained as:

$$\frac{\partial}{\partial x}\delta(x,y,z)]_{(x=\pm\frac{g_x}{2})} = \pm\frac{S_g}{2D^*}\delta(\pm\frac{g_x}{2},y,z) \quad \dots \quad (7)$$

$$\frac{\partial}{\partial y}\delta(x,y,z)]_{(y=\pm\frac{g_y}{2})} = \pm\frac{S_g}{2D^*}\delta(x,\pm\frac{g_y}{2},z) \quad \dots \quad (8)$$

S_g denote the recombination velocity at grain boundaries.

Imposing the boundary conditions on the governing transport equations yields two transcendental relations from which the coefficients can be determined. C_k and C_j can be extracted, either by graphical root finding or via a numerical solver. These relations are given by:

$$\tan C_j\frac{g_x}{2} = \frac{1}{C_j}\times\frac{S_g}{2D*} \quad \dots \quad (9)$$

$$\tan C_K(B)\frac{g_y}{2} = \frac{1}{C_k(b)}\times\frac{S_g}{2D*} \quad \dots \quad (10)$$

Substituting the general solution into the continuity equation yields:

$$\frac{\partial^2}{\partial z^2}Z_{j.k}(z) - \frac{Z_{j.k}(z)}{{L^*_{j.k}}^2} = \frac{-G(z)}{D^*_{j.k}} \quad \dots(11)$$

With

$$\frac{1}{L^2_{j.k^2}} = C_j^2 + C_k^2 + \frac{1}{L^{*2}} \quad \dots \quad (12)$$

$$\frac{1}{D^*_{j.k}} = \frac{16\sin(C_j\frac{g_x}{2})\sin(C_k(B)\frac{g_y}{2}}{D^*[C_j g_x + \sin(C_j g_x)][C_k(B)g_y + \sin(C_k(B)g_y)]} \quad \dots \quad (13)$$

$L^*_{j,k}$ and $D^*_{j,k}$ Represent the effective diffusion length and the effective diffusion coefficient, respectively [3].

The solution to this equation (11) is:

$$Z_{j.k}(z) = A_{j.k}\sinh\frac{z}{L^*_{j.k}} + B_{j.k}\cosh\frac{z}{L^*_{j.k}} + \sum_{i=1}^{3} k_j e^{-b_i z} \quad \dots \quad (14)$$

with:

$$K_i = -\frac{n}{D^*_{j.k}}\frac{a_i {L^*_{j.k}}^2}{{b_i}^2{L^*_{j.k}}^2 - 1} \quad \dots \quad (15)$$

The constants $A_{j,k}$ and $B_{j,k}$ are determined from the boundary conditions at the junction and the rear surface as follows:

Published By:
Blue Eyes Intelligence Engineering
and Sciences Publication (BEIESP)

$$D^* \frac{\partial}{\partial z}\delta(x,y,z) = S_f \delta(x,y,z) \quad \text{for z=0} \quad \ldots \quad (16)$$

$$D^* \frac{\partial}{\partial z}\delta(x,y,z) = -S_b \delta(x,y,z) \quad \text{for z=H} \quad \ldots \quad (17)$$

S_f denote the effective front-side recombination velocity, written as the sum of two components,

S_b is the recombination velocity at the rear surface of the solar cell.

$$S_f = S_{f0} + S_{fj} \quad \ldots \quad (18)$$

Here, S_{f0} is the intrinsic junction term associated with the shunt pathway (R_{sh}) at the junction [4], while S_{fj} captures the load-driven carrier flux imposed by the external circuit and thus sets the operating point of the cell [4]. Sb denotes the effective recombination velocity at the rear surface of the solar cell. Assessing how an external magnetic field influences the photovoltage in polycrystalline silicon devices is essential for performance optimization. By imposing a Lorentz force on electrons and holes, the field perturbs carrier trajectories and generally reduces the effective diffusion length, especially when lifetimes are extended. The resulting change in photovoltage depends on device geometry and illumination mode (front, rear, or bifacial), as documented in studies of surface/recombination control and bifacial operation [3]. Our simulation framework solves the classical semiconductor transport equations while allowing the diffusion coefficient D and diffusion length L to vary with magnetic field, following standard device physics and magnetic-transport formulations reported in [4]. Within this idealized model, surface-passivation effects are not treated explicitly and are assumed to play a negligible role in carrier collection [2]. Before discussing the primary outcomes, we delineate the field-intensity window over which magnetic effects become significant: Figures 2 and 3 chart the dependencies D(B) and L(B), respectively, thereby defining the relevant operating range used in the subsequent simulations [4].

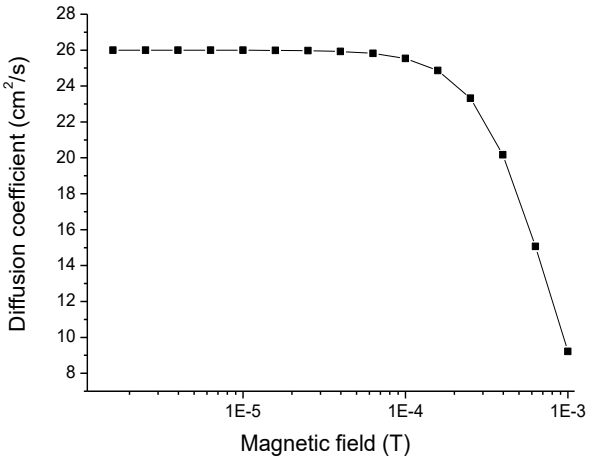

[Fig.2: Variation of the Carrier Diffusion Coefficient with Magnetic Field Intensity]

For $B \lesssim 10 - 4\,T$, the diffusion coefficient is essentially unchanged at $\sim 25\,cm^2.s^{-1}$. Once B exceeds this level, D falls sharply, reaching. $\sim 10\,cm^2.s^{-1}$, consistent with a substantial reduction of the effective mobility μ via the Einstein relation $D = \mu kT/q$.D.

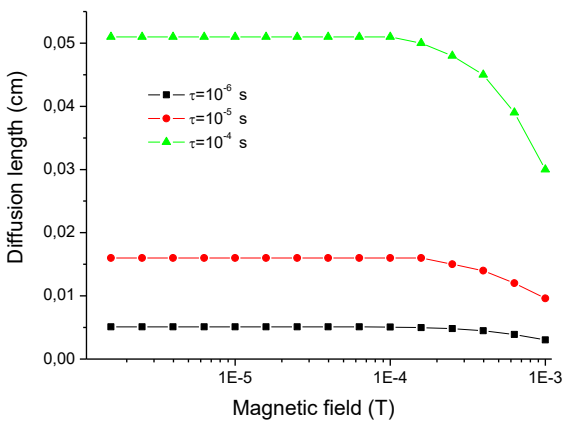

[Fig.3: Evolution of the Diffusion Length as a Function of Magnetic Field, for Different Carrier Lifetimes]

Because $L \propto \sqrt{D\tau}$, longer carrier lifetimes naturally yield longer diffusion lengths. Yet for magnetic fields below about 1e−4 T, L is effectively insensitive to B; an apparent reduction emerges only once B exceeds this threshold, and the effect is most evident for long- τ carriers. These preliminary trends guided our operating window: we concentrate on $B = 1e - 4\,T$, where transport coefficients, and thus the photovoltage, respond measurably. At fields $< 10 - 4\,T$, the perturbations to mobility/diffusion remain within numerical scatter and translate into negligible changes in V_{ph}; within $1e - 4$ to $1e - 3T$, the magnetic influence is strong enough to reveal the coupling between magnetic perturbations and transport phenomena. Accordingly, the simulations that follow examine the combined impact of B and base thickness on the photovoltage, using this field range to quantify the device's magnetic susceptibility and to anticipate potential performance drifts under realistic industrial or environmental conditions.

B. Expression of the Photogenerated Current Density J_{ph} (in A.cm⁻²)

The general expression of the photogenerated current density under illumination mode m ∈ {Front, Rear, dual} is given by:

$$j_{ph.m} = \frac{qD^*}{g_x g_y} \int_{-\frac{g_x}{2}}^{\frac{g_x}{2}} \int_{\frac{g_y}{2}}^{\frac{g_y}{2}} \left[\frac{\partial}{\partial z}\delta(x,y,z)\right]_{z=0} dxdy \quad \ldots \quad (19)$$

where:

- $J_{ph,m}$: photogenerated current density for illumination mode mmm (A·cm⁻²),
- q: elementary charge of the electron (1,602 10 e−19 C),
- D^* : effective diffusion coefficient under the influence of the magnetic field (cm²/s),
- g_x, g_y: lateral dimensions of the simulation domain along the x and y directions (in cm),

$\delta_m(x,y,z)$ excess minority carrier density induced by optical generation for mode m, $\left[\frac{\partial}{\partial z}\delta_m\right]_{z=0}$: derivative of the excess carrier density evaluated at the junction plane (z = 0).

Published By:
Blue Eyes Intelligence Engineering
and Sciences Publication (BEIESP)

C. Expression of the Photovoltage (in V)

The general expression for the photovoltage under illumination mode m ∈ {Front, Rear, Dual} is given by:

$$V_{ph_m} = V_T \ln\left(1 + \frac{1}{n_0}\int_{-\frac{gx}{2}}^{\frac{gx}{2}}\int_{-\frac{gy}{2}}^{\frac{gy}{2}} \delta_m(x,y,0)dxdy\right) \quad \ldots \quad (20)$$

With

$$V_T = \frac{KT}{q} \quad \ldots \quad (21)$$

And

$$n_0 = \frac{{n_i}^2}{N_b} \quad \ldots \quad (22)$$

Where:

1). $V_{ph,m}$: Photovoltage for illumination mode m (V),
2). V_T: Thermal voltage
3). K: Boltzmann constant
4). T: Absolute temperature (K)
5). q: elementary charge of the electron (1,602. e−19 C),
6). n_0: Reference equilibrium minority carrier concentration (cm^{-3})
7). ${n_i}^2$: Intrinsic carrier concentration squared (cm^{-6})
8). N_b: Base doping concentration (cm^{-3})
9). D^*: effective diffusion coefficient under the influence of the magnetic field (cm^2/s),
10). g_x, g_y: lateral dimensions of the simulation domain along the x and y directions (in cm),
11). $\delta_m(x,y,z)$: excess minority carrier density induced by optical generation for mode m,
12). $\left[\frac{\partial}{\partial z}\delta_m\right]_{z=0}$: derivative of the excess carrier density evaluated at the junction plane ($z = 0$)

D. Expression of the Series Resistance (in Ω.cm²)

Figure 4 displays a J-V characteristic; the encircled region corresponds to the quasi-vertical segment, indicating a weak dependence on photocurrent density. This feature is observed across all curves obtained with other parameter sets, regardless of the illumination mode. In this regime, the device behaves like a voltage source, delivering an almost constant value equal to the open-circuit photovoltage V_{oc}. In a real cell, non-idealities arise: a parasitic series resistance R_s, in series with the ideal source (emf ≈V_{oc}), causes a voltage drop under load and accounts for the deviation from verticality as the current increases (high-voltage slope).

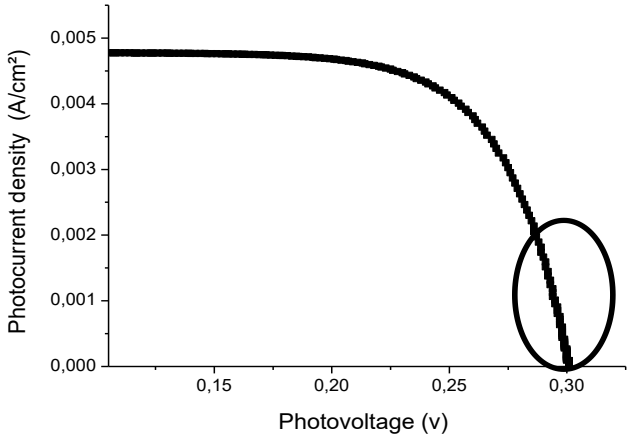

[Fig.4: J-V Characteristic of a Silicon Solar Cell]

Figure 5 presents the equivalent electrical circuit of a silicon solar cell operating in this regime.

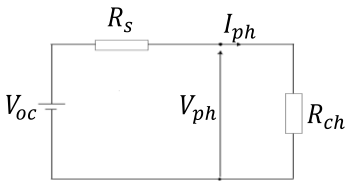

[Fig.5: Equivalent Electrical Circuit of the Solar Cell Under Open-Circuit Conditions]

V_{oc}.: open-circuit photovoltage
R_s: series resistance
J_{ph}: photocurrent
V_{ph}: photovoltage
R_{ch}: minimal load resistance

Figure 5 shows an equivalent electrical circuit of a solar cell under open-circuit conditions.

Applying Kirchhoff's voltage law to this circuit, we obtain the following relation:

$$V(s_f) = V_{co} - R_s.I_{ph}(S_f) \quad \ldots \quad (23)$$

Which leads to the following relation:

$$R_s = \frac{V_{co} - V(S_f)}{I_{ph}(S_f)} \quad \ldots \quad (24)$$

III. RESULTS AND DISCUSSION

In this work, we investigate bifacial polycrystalline silicon solar cells subjected to a modest external magnetic field B=1e-4 to 1e-3T. We analyze the photovoltage, photocurrent density, and the series resistance R_s as functions of carrier collector velocity (CCV), base thickness (e=100 -400 µm) and illumination mode (front, rear, and dual), primarily in the near–open-circuit regime.

Figures (6) and (7) show the J_{ph}-V_{ph} curves for varied magnetic fields B, with base thicknesses of 100 µm and 300 µm, respectively.

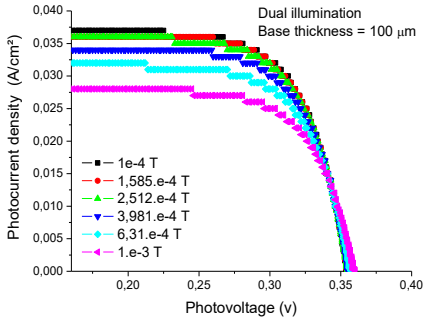

[Fig.6: Photocurrent Density as a Function of Photovoltage for Different Magnetic-Field Values]

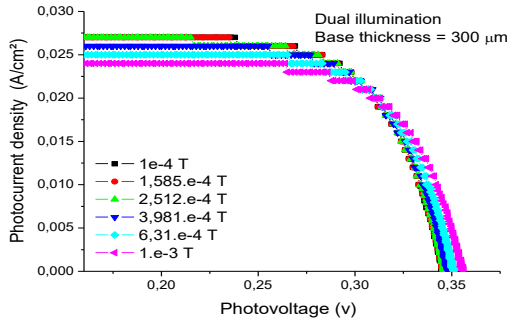

[Fig.7: Photocurrent Density as a Function of Photovoltage for Different Magnetic-Field Values]

Under dual illumination, the $J_{ph} - V_{ph}$ curves for base thicknesses of 100 µm (Fig. 6) and 300 µm (Fig. 7), subjected to increasing magnetic fields from 1e-4 T to 1e−3 T, show:

i) a decrease in short-circuit photocurrent density from 0.037 to 0.027 $A \cdot cm^{-2}$ ($\approx 27\%$) for 100 µm and from 0.027 to 0.024 $A \cdot cm^{-2}$ ($\approx$ 11%) for 300 µm, and

ii) a slight rise of the open-circuit photovoltage above 0.35 V, at low V_{ph}, J_{ph} remains maximal ($\approx J_{sc}$) and then decreases rapidly to zero at V_{oc}.

This trend can be explained by Lorentz-force deflection of carriers, an effective reduction of the diffusivity D and of the diffusion length $L = \sqrt{D\tau}$, as well as an apparent increase in the series resistance R_s, mechanisms that degrade carrier collection, in qualitative agreement with experimental observations and magneto-transport modelling on Si cells/modules [5]. The relatively stronger attenuation for 100 µm than for 300 µm is consistent with the existence of a magnetic-field-dependent optimal base thickness [6], while the orientation of B relative to the carrier flux can modulate the magnitude of the degradation [7]. To explain in detail the variations of V_{ph} observed near open circuit, it is therefore essential to investigate the dependence of the series resistance on base thickness and magnetic field, $R_s(e, B)$, via a parametric extraction from the $J - V$ curves (in parallel with J_0, n, and R_{sh}): under magnetic bias, magnetoresistance and transport modifications can render R_s non-negligible even in the high-voltage region, thereby clarifying the slight evolution of V_{oc} and the limitation of carrier collection, this is precisely the objective of the present work. In the next section, we will present the $J - V$ characteristics as a function of base thickness for the three illumination modes (front, rear, and dual) at a fixed magnetic field $B = 1e - 4$ T.

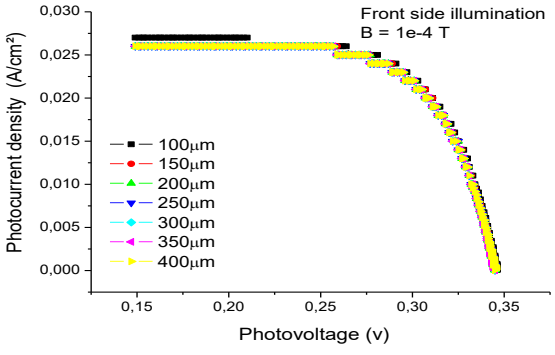

[Fig.8: Photocurrent Density as a Function of Photovoltage for Various Base Thicknesses Under Front-Side Illumination]

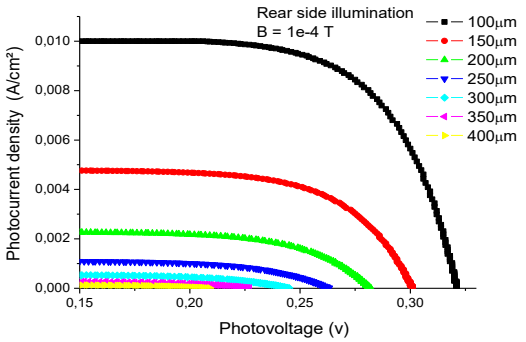

[Fig.9: Photocurrent Density as a Function of Photovoltage for Various Base Thicknesses Under Rear-Side Illumination]

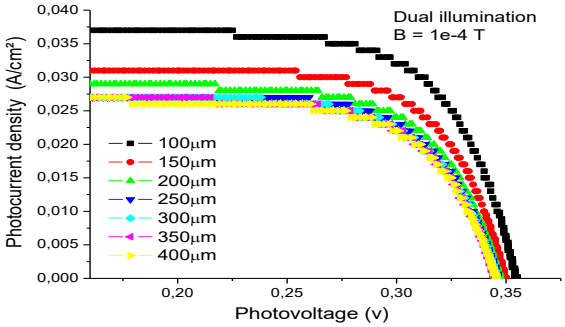

[Fig.10: Photocurrent Density as a Function of Photovoltage for Various Base Thicknesses Under Dual Illumination]

With the magnetic field fixed at $B = 1e - 4$ T, the $J_{ph} - V_{ph}$ curves obtained under front illumination (Fig. 8), rear illumination (Fig. 9), and dual illumination (Fig. 10) show that the base thickness has only a weak influence in front illumination, because the junction is on the illuminated side, carrier collection remains efficient as long as the diffusion length exceeds the active base thickness and back-surface reflection increases the effective optical path length. By contrast, under rear illumination, photogeneration occurs far from the junction; collection then becomes sensitive to the pair (e) and to the surface recombination velocities (SRV), which degrade J_{ph} and V_{ph} as e increases. Under dual illumination, generation co-occurs on both sides, improving both current and voltage. In our data, we observe J sub sc almost equal to 0.037 A/cm^2 and V sub oc asymptotically equal to 0.35 V, in line with the bifacial literature [8]. The fact that $e = 100$ µm offers the best trade-off is consistent with an optimal thickness determined by surface properties: with effective passivation (low SRV), thinning can raise V_{oc} while maintaining high J_{sc} up to a maximum before optical losses set in; when SRV are higher, increasing e mainly enhances recombination and penalizes performance [9]. In all three modes, J_{ph} remains maximal and nearly flat at low V_{ph} ($\approx J_{sc}$), then falls rapidly to zero at V_{oc}. To interpret the trends near open circuit in detail, it is necessary to analyze the dependence of the series resistance on thickness (and, more generally, on magnetic, open parenthesis e, B close parenthesis, via parametric extraction from the J minus V curves (alongside J sub 0, n, and R sub sh); indeed, the high-voltage slope and the

apparent V sub oc are well known to be sensitive to R sub s.

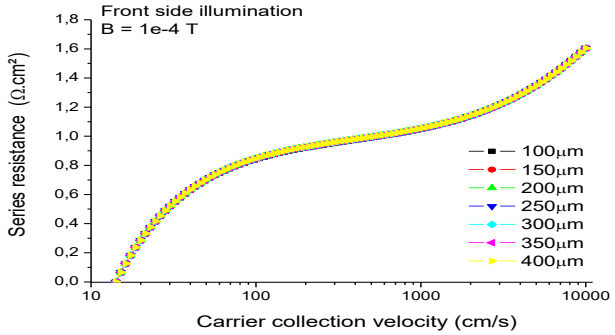

[Fig.11: Series Resistance as a Function of Carrier-Collection Velocity for Various Base Thicknesses Under Front-Side Illumination, with $B = 1e-4\,T$]

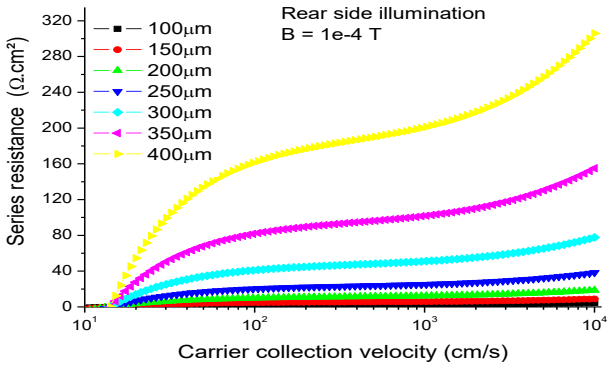

[Fig.12: Series Resistance as a Function of Carrier-Collection Velocity for Various Base Thicknesses Under Rear-Side Illumination, with $B = 1e-4\,T$]

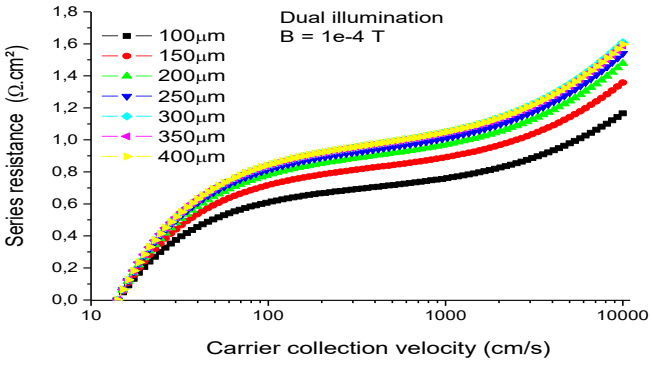

[Fig.13: Series Resistance as a Function of Carrier-Collection Velocity for Various Base Thicknesses Under Dual Illumination, with $B = 1e-4\,T$]

With the magnetic field fixed at $B = 1e-4\,T$, the $R_s - CCV$ (carrier collection velocity) curves under front illumination (Fig. 11), rear illumination (Fig. 12), and dual illumination (Fig. 13) show that, for front illumination, varying the base thickness e scarcely affects the series resistance, which remains low ($\sim 1.6\ \Omega.cm^{-2}$), consistent with collection near the junction and reduced ohmic pathways. Under rear illumination, where photogeneration is displaced from the intersection, R_s becomes strongly dependent on e and CCV: longer conduction paths in the base and lower local injection increase the apparent resistance extracted from the high-voltage slope, reaching tremendous values (up to $\sim 320\,\Omega\cdot cm^{-2}$ in our data); under dual illumination, the more symmetric generation mitigates these limitations and keeps R_s low ($\approx 1.6\ \Omega\cdot cm^{-2}$). These trends align with:

i) the classical decomposition of R_s (sheet, spreading/diffusion in the base, contact and metallization resistances) and its injection dependence $R_s(J)$, which makes the "apparent R_s" increase as CCV (and thus current) rises, and

ii) experimental evidence of the distributed, local character of R_s from electroluminescence and thermography, showing that illumination and geometry modulate resistive pathways.

The increase of R_s with e across CCV is expected, since bulk and sheet contributions grow with adequate base thickness when not compensated by doping/passivation; conversely, dual illumination raises injection on both sides and lowers the "apparent R_s"

Finally, under rear illumination, the series resistance is minimal for $e = 100$ and $150\,\mu m$ compared with higher thicknesses, and this holds across all CCV values considered. This $R_s(e) - CCV$ profile, combined with the longer collection path and the increase in bulk and surface recombination as e grows, directly explains the trends previously observed on the $J - V$ curves under rear illumination: the photocurrent density and the photovoltage drop sharply with thickness, decreasing from about $10\,mA.cm^{-2}$ and $0.34\,V$ at $e = 100\,\mu m$ to $\approx 0\ mA\cdot cm^{-2}$ and $0.23\,V$ at $e = 400\,\mu m$. More specifically, the decrease of J_{sc} as e increases (generation far from the junction, diffusion length L comparable to or smaller than e) together with a concomitant rise in the saturation current J_0 lead, via $V_{oc} \approx (nkT/q)\ln(J_{sc}/J_0 + 1)$, to a reduction in V_{oc}; the growth of R_s with e further steepens the high-voltage slope and can bias the "apparent" V_{ph} extracted near open circuit (underestimation depending on the extraction method and the voltage range). This underscores the need for a joint extraction $\{J_0, n, R_s, R_{sh}\}$ and for analyses separated by illumination mode and by CCV [10] which will undoubtedly be considered in our future work.

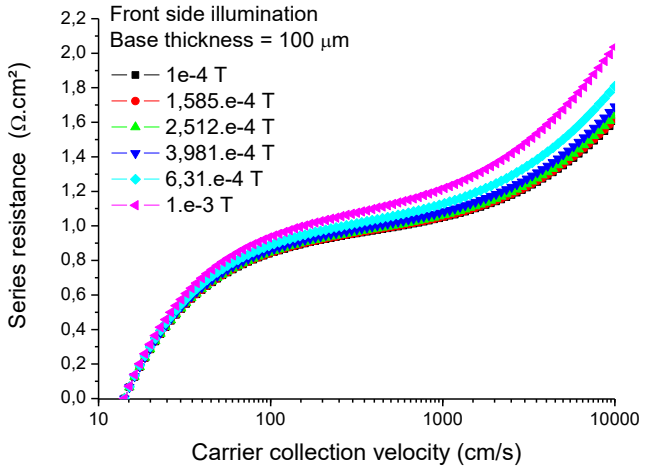

[Fig.14: Series Resistance as a Function of Carrier-Collection Velocity for Different Magnetic-field Values B, Under Front-Side Illumination, at a Base Thickness of $e = 100\,\mu m$]

Published By:
Blue Eyes Intelligence Engineering
and Sciences Publication (BEIESP)

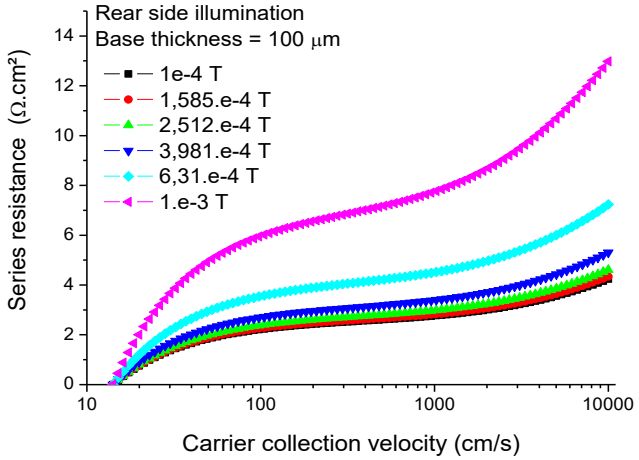

[Fig.15: Series Resistance as a Function of Carrier-Collection Velocity for Different Magnetic-Field Values B, Under Rear-Side Illumination, at a base Thickness of $e = 100$ µm]

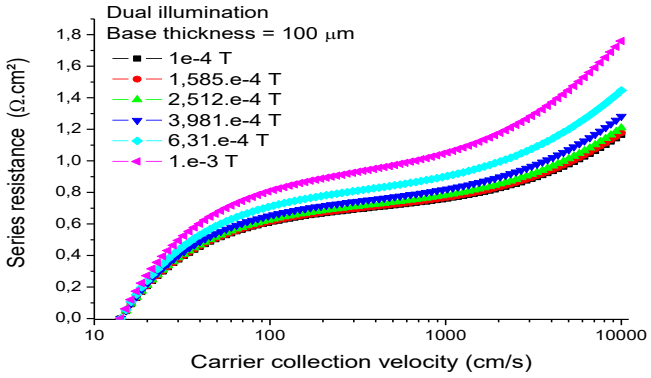

[Fig.16: Series Resistance as a Function of Carrier-Collection Velocity for Different Magnetic-Field Values B, Under Dual Illumination, at a Base Thickness of $e = 100\,\mu m$]

With the magnetic field $B \in [1e-4, 1e-3]$ T, the $R_s - CCV$ curves exhibit a monotonic increase of R_s as both CCV and B increase, regardless of illumination mode. However, this rise is markedly more moderate under front and dual illumination than under rear illumination: in our data, the maximum. R_s under rear illumination is 7.77× that under dual illumination and 6.36× that under front illumination. The lower R_s values under dual illumination (relative to front illumination) at $e = 100$ µm can be attributed to:

i) bilateral generation that shortens the mean collection distance and thus the lateral paths in the emitter and in the base (a more minor spreading component),

ii) more homogeneous injection that increases photoconductivity (lower effective resistivity) and reduces current crowding at the contacts, and

iii) a more symmetric current distribution that reduces ohmic drops in the metallization [11].

The influence of the magnetic field amplifies these contrasts: under rear illumination, the combination of a longer collection path and Lorentz-force deflection of carriers increases the effective resistivity (magnetoresistance) and the "apparent" R_s extracted from the high-voltage slope; the impact is intermediate under dual illumination and weaker under front illumination [12]. These observations are consistent with the classical decomposition of R_s (sheet, spreading/base, contact, and metallization resistances) and with the dependence of R_s on the injection level and the magnetic field [13].

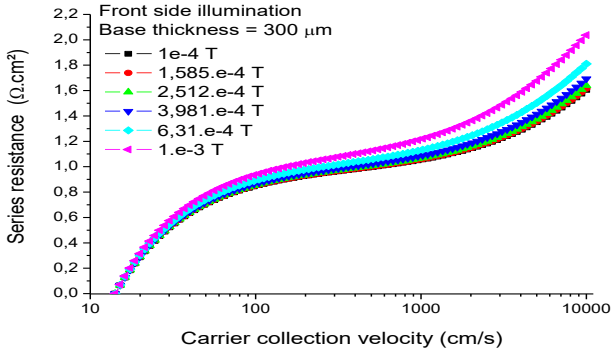

[Fig.17: Series Resistance as a Function of Carrier-Collection Velocity for Different Magnetic-Field Values B, Under Front-Side Illumination, at a Base Thickness of $e = 300\,\mu m$]

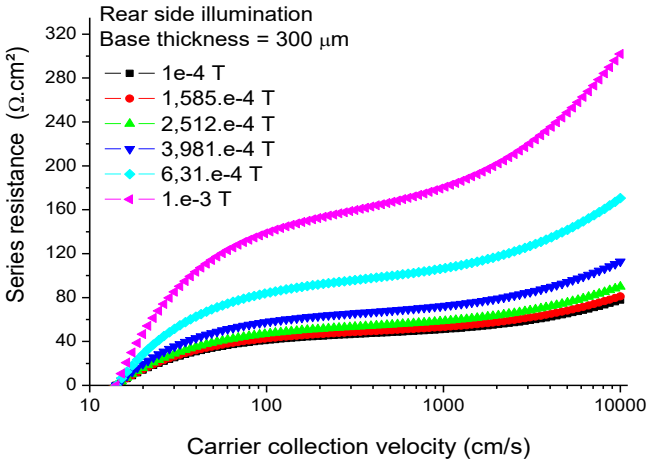

[Fig.18: Series Resistance as a Function of Carrier-Collection Velocity for Different Magnetic-Field Values B, Under Rear-Side Illumination, at a base Thickness of $e = 300\,\mu m$]

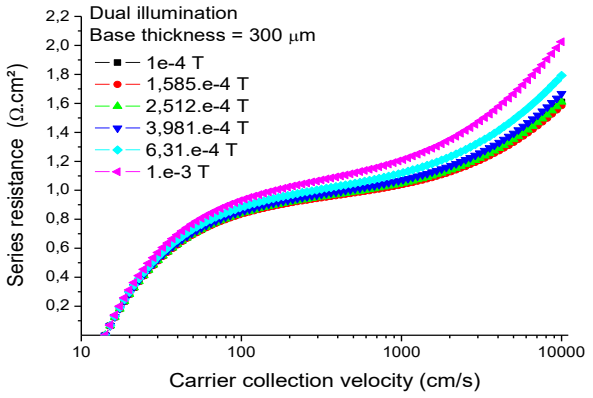

[Fig.19: Series Resistance as a Function of Carrier-Collection Velocity for Different Magnetic-Field Values B, Under Dual Illumination, at a Base Thickness of $e = 300\,\mu m$]

Under $B \in [1e-4, 1e-3]$ T, the $R_s - CCV$ curves at $e = 300$ µm show that R_s increases with CCV and with B, regardless of illumination mode, consistent with the known sensitivity of

the "apparent" R_s to the injection level and to the high-voltage slope of the $J-V$ curves. For front and dual illumination, this rise remains moderate, and R sub s stays low (tilde operator 2.2 cap omega. and $R_s$stays low ($\sim 2.2\,\Omega.\mathrm{cm}^{-2}$), with curves very similar to those obtained at $e = 100\,\mu m$. Still at $e = 300\,\mu m$, the R_s values under rear illumination are $> 20\times$those recorded at $e = 100\,\mu m$ and $> 140\times$those of the other two illumination modes for the same thickness, which is explained by longer spreading paths in the base and by an R_s extraction that is more penalized near open circuit. The increase with B accentuates these contrasts: Lorentz-force deflection reduces the mobility $\mu(B)$and, via the Einstein relation, the diffusion coefficient $D(B) = \mu(B)kT/q$; the effective conductance drops, which increases the resistivity and the apparent R_s [13]. This magnetoresistance mechanism, observed experimentally in Si cells/modules under field, leads to increased current and voltage losses, especially when generation is far from the junction (rear illumination) [13]. Finally, the tremendous R_s values inferred under rear illumination should be interpreted with caution: voltage-dependent electroluminescence and lock-in thermography show that R_s is local/distributed and that resistive paths (sheet, spreading in the base, contacts, and metallization) vary with illumination and geometry; some extraction methods can under- or over-estimate the "apparent" R_s depending on the voltage region analyzed.

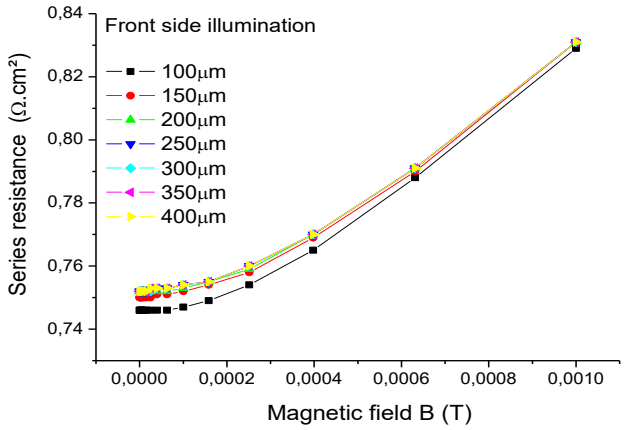

[Fig.20: Series Resistance as a Function of Magnetic Field B, Under Front-Side Illumination, for Various Base Thicknesses]

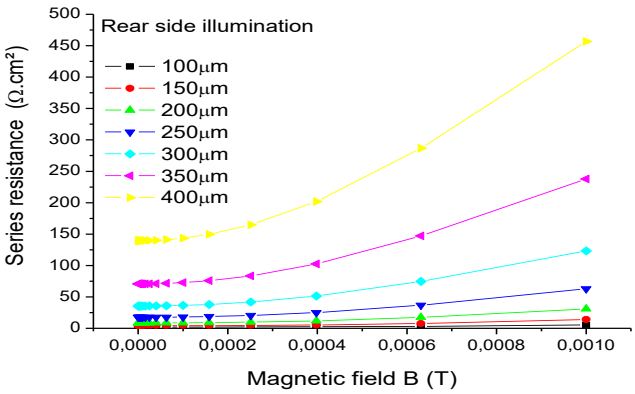

[Fig.21: Series Resistance as a Function of Magnetic Field B, Under Rear-Side Illumination, for Various Base Thicknesses]

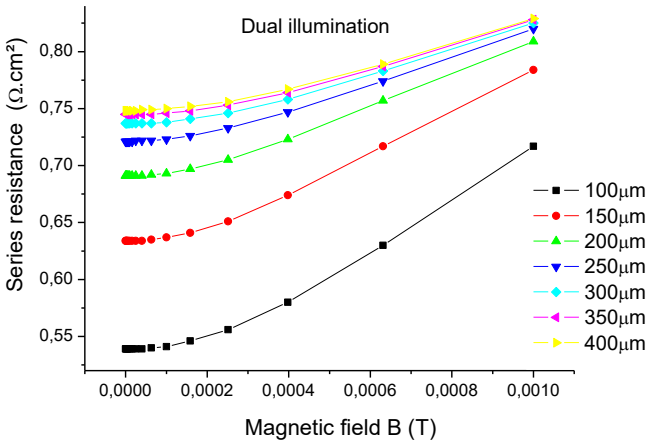

[Fig.22: Series Resistance as a Function of Magnetic Field B, Under Dual Illumination, for Various Base Thicknesses]

Under a variable magnetic field B (here $1e-4$ to $1e-3\,T$), the $R_s(B)$ plots reveal a systematic increase in series resistance as B grows, for all illumination modes and all base thicknesses considered. The magnitude of this increase depends strongly on the base thickness e and on the illumination mode: under rear illumination, where photogeneration is far from the junction, R_s reaches the highest values; it remains more moderate under front and dual illumination, the latter benefiting from bilateral generation that shortens the mean collection distance and relieves resistive-path congestion (sheet, base, metallization). Physically, the field effect can be interpreted as magnetoresistance: the Lorentz force reduces the effective mobility $\mu(B)$ and, via the Einstein relation, the diffusion coefficient $D(B) = \mu(B)\,kT/q$; in the Drude approximation, when $B \perp J$, the longitudinal component follows $D^*(B) = D/(1+(\mu B)^2)$, leading to a shortening of $L^*(B) = \sqrt{D^*.\tau}$ and a drop in conductance that appears as an increase in the "apparent" R_s [12]. In parallel, a thicker base increases the spreading contribution within the base and lengthens ohmic paths; under rear illumination, this effect combines with bulk/surface recombination along a longer collection path, explaining the high R_s values and their sensitivity to B. The orientation of the field with respect to the carrier flux can further modulate the observed magnitude [7]. These trends are consistent with the classical decomposition of R_s (sheet, base spreading, contact, and metallization resistances) and with the effects of the injection level and the magnetic field on the high-voltage slope of the $J-V$ curves [12].

With CCV = 60.256 cm·s⁻¹, the curves below depict the maximum absolute change in series resistance, ΔR_s (in $\Omega.\mathrm{cm}^{-2}$), over the magnetic-field range $B = 1e-4$ to $1e-3\,T$, plotted as a function of base thickness e and for different illumination modes.

Retrieval Number: 100.1/ijitee.J1142140100925
DOI: 10.35940/ijitee.J1142.14100925
Journal Website: www.ijitee.org

Published By:
Blue Eyes Intelligence Engineering and Sciences Publication (BEIESP)

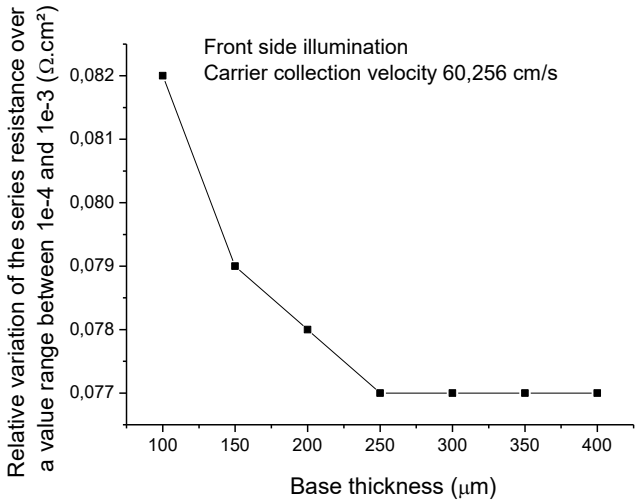

[Fig.23: Absolute Change in Series Resistance as a Function of Base Thickness Over the Magnetic-Field Range $B = 1e-4$ *to* $1e-3\,T$, Under Front-Side Illumination]

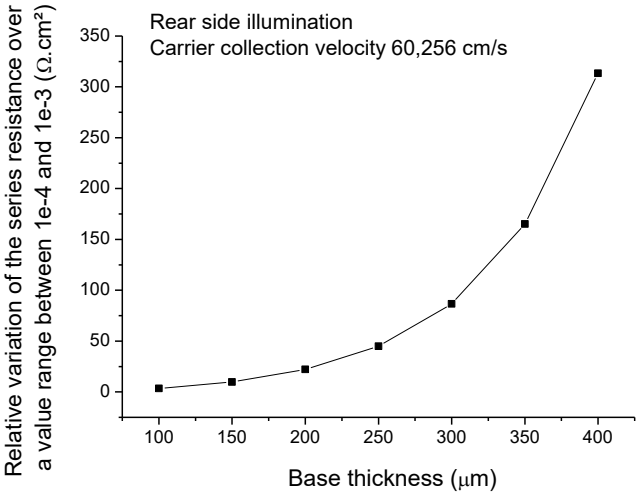

[Fig.24: Absolute Change in Series Resistance as a Function of Base Thickness Over the Magnetic-Field Range $B = 1e-4$ *to* $1e-3\,T$, Under Rear-Side Illumination]

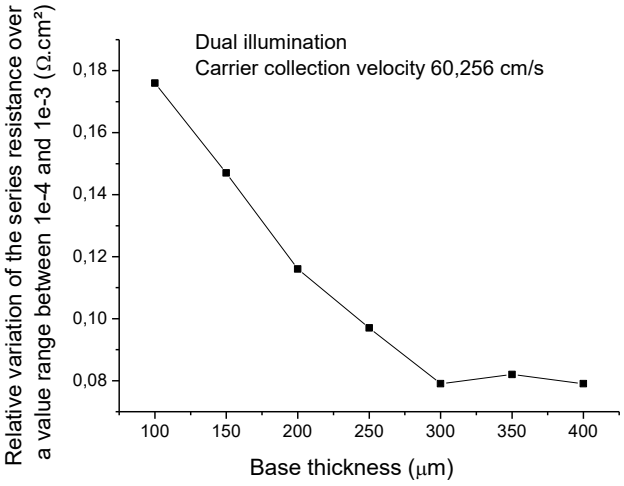

[Fig.25: Absolute Change in Series Resistance as a Function of Base Thickness Over the Magnetic-Field Range $B = 1e-4$ *to* $1e-3\,T$, Under Dual Illumination]

Under front illumination and dual illumination, ΔR_s shows a slight increase as e decreases, which can be explained by:

i) A reweighting of the R_s components toward sheet/contact resistances when the base-spreading contribution becomes marginal at small e, and/or

ii) Extraction effects near high voltage, where the slope dV/dJ may be partly dominated by recombination, biasing the estimate of ΔR_s (method and voltage window) [14].

By contrast, under rear illumination, ΔR_s decreases as e decreases, consistent with shorter spreading paths and lower effective resistivity in the base when generation occurs far from the junction: thinning reduces the collection distance and limits the internal ohmic drop. At this fixed CCV level, note that, in general, the "apparent" R_s increases with injection level (more current ⇒ a larger $J.R_s$ drop in the high-voltage region), a point to keep in mind when interpreting ΔR_s trends.

IV. CONCLUSION

In conclusion, our results show that applying a modest magnetic field (B = 1e-4 to 1e-3 T) systematically increases the series resistance R_s and amplifies losses near the open circuit, with maximum sensitivity under rear illumination, mitigated under dual illumination, and more moderate under front illumination. Increasing the base thickness degrades carrier collection under rear illumination (marked decreases in Jsc and Voc), whereas dual illumination shortens the mean collection distance and limits the "apparent" Rs. A magnet ore sistive interpretation (reduction of μ, and hence of D and L) accounts for the overall trend; however, at millitesla fields, the direct changes in diffusion remain small, emphasising the dominant roles of surfaces/contacts, extraction geometry, and injection effects. Joint parametric extraction of {J_0, n, R_s, Rsh}, performed by illumination mode and thickness, is essential to resolve the high-voltage slopes and connect transport to performance. These insights provide design guidelines (thickness selection, passivation, contact engineering, illumination strategy); the effects of field orientation and temperature, together with local mapping of R_s, will be addressed in our future work.

may review the main points of the paper, but do not replicate the abstract as the conclusion. A conclusion might elaborate on the importance of the work or suggest applications and extensions.

DECLARATION STATEMENT

After aggregating input from all authors, I must verify the accuracy of the following information as the article's author.

- **Conflicts of Interest/ Competing Interests:** Based on my understanding, this article has no conflicts of interest.
- **Funding Support:** This article has not been funded by any organizations or agencies. This independence ensures that the research is conducted with objectivity and without any external influence.

- **Ethical Approval and Consent to Participate:** The content of this article does not necessitate ethical approval or consent to participate with supporting documentation.
- **Data Access Statement and Material Availability:** The adequate resources of this article are publicly accessible.
- **Author's Contributions:** Each author has individually contributed to the article. Moussa Toure: data analysis, writing, original draft preparation, review and editing, Mamadou Lamine Samb: Conceptualisation, experiment, data analysis, supervision, writing-original draft preparation, review and editing, Youssou Gning: review and editing, Aly Toure: review and editing, Ahmed Mohamed-Yahya: Conceptualisation, experiment, data analysis, supervision, review and editing,

REFERENCES

1. Liu, S., Zhang, M., & Wang, X. (2019). Enhanced Bifacial Solar Cell Performance through 3D Modelling. Renewable Energy, 135, 1427–1434. DOI: https://doi.org/10.1016/j.renene.2018.12.062
2. Thiaw, C, et al., "Determination of the optimal base thickness of an n+–pp+ silicon solar cell under magnetic field," J. Electromagn. Anal. Appl., vol. 12, no. 7, pp. 139–154, 2020. DOI: https://doi.org/10.4236/jemaa.2020.127009
3. TOURE, M, et al, "3D Mathcad Simulation of Photovoltage in C-Si Solar Cells Under Multispectral Illumination: Combined Effect of Transverse Magnetic Field and Base Thickness", DOI: https://doi.org/10.5281/zenodo.17007121
4. Zoungrana, M., et al., "The effect of magnetic field on the efficiency of a silicon solar cell under an intense light concentration", Advances in Science and Technology Research Journal Volume 11, Issue 2, June 2017, pages 133–138. DOI: https://doi.org/10.12913/22998624/69699
5. Ndeto, M. P, Wekesa, D. W, Kinyua, R, & Njoka, F. (2020). Investigation into the effects of the Earth's magnetic field on the conversion efficiency of solar cells. Renewable Energy, 159, 184–194. DOI: https://doi.org/10.1016/j.renene.2020.05.143
6. Faye, D., et al. (2020). Lamella Silicon Solar Cell under Both Temperature and Magnetic Field: Width Optimum Determination. Journal of Electromagnetic Analysis and Applications, 12, 43–55. DOI: https://doi.org/10.4236/jemaa.2020.124005
7. Sourabié, I, Zerbo, I, Zoungrana, M, Combari, D. U, Bathiebo, D. J, (2017). Effect of Incidence Angle of Magnetic Field on the Performance of a Polycrystalline Silicon Solar Cell under Multispectral Illumination. Smart Grid and Renewable Energy, 8, 325–335. DOI: https://doi.org/10.4236/sgre.2017.810021
8. Liang, T. S, et al. "A review of crystalline silicon bifacial photovoltaic performance characterisation and simulation," Energy Environ. Sci. 12 (2019) 116–148. DOI: https://doi.org/10.1039/C8EE02184H
9. Lin, C.-H, "The Effect of Thickness and Surface Recombination Velocities on the Performance of Silicon Solar Cell," Solids 6 (2025) 33. DOI: https://doi.org/10.3390/solids6030033
10. Wagner, J.-M, et al. "A critical review… Rs, dark vs. Rs, light?" AIP Conf. Proc. 1999 (2018) 020022. DOI: https://doi.org/10.1063/1.5049261
11. Guerrero-Lemus, R, et al. "Bifacial solar photovoltaics – A technology review," Renew. Sustain. Energy Rev. 60 (2016) 1533–1549. DOI: https://doi.org/10.1016/j.rser.2016.03.041
12. Fathabadi, H (2020). Magnetic field effect on silicon-based solar cells. Materials Chemistry and Physics, 244, 122684. DOI: https://doi.org/10.1016/j.matchemphys.2020.122684
13. Combari, D. U., et al. (2018). Performance Investigation of a Silicon Photovoltaic Module under the Influence of a Magnetic Field. Advances in Condensed Matter Physics, 2018, Article ID 6096901. DOI: https://doi.org/10.1155/2018/6096901
14. Tada, K, et al. "What do apparent series and shunt resistances in solar cells really mean?" Phys. Status solidi (a) 215 (2018) 1800448. DOI: https://doi.org/10.1002/pssa.201800448

AUTHOR'S PROFILE

Moussa Toure, Doctor of Materials Science from Assane Seck University in Ziguinchor, Senegal. Senegal. I am a lecturer and researcher at Iba Der Thiam University in Thiès, Senegal. I have published articles on a new method of doping silicon, on the development and characterization of silicon nanostructures. I have also published articles on inorganic perovskites, on the possibility of using heterostructures of silicon carbides on silicon (3C-SiC/Si) for photovoltaic applications. I have also published articles on finite element modelling of a solar cooker: temperature and fluid velocity distributions, the summation of silicon carbide-based solar cells (3C-SiC/Si). I am now interested in the improvements to be made within the solar cell, first in simulation and then experimentally.

Mamadou Lamine SAMB is an Associate Professor in Applied Physics, specialized in Electronics and Renewable Energies. He has been the Head of the Physics and Chemistry Department at the University Iba Der Thiam of Thiès (UIDT) since 2020. He also currently serves as the Scientific Coordinator of the Master's program in Physics, Chemistry, and Applications (PCA). His research focuses on the numerical modelling of semiconductor devices, the simulation of thin-film transistors (TFTs) manufactured at very low temperatures, and the optimisation of photovoltaic cells. He is also interested in hybrid energy systems and energy efficiency. From 2015 to 2021, he was the Head of the Physics and Chemistry Bachelor's program at UIDT, which he contributed to establishing and developing. He was also a member of the Internal Quality Assurance Unit of the UFR-SET. Mamadou Lamine SAMB has extensive experience in student supervision and scientific mentoring. He leads research projects and supervises final-year theses in the fields of electronics, renewable energies, and energy efficiency. His work contributes to the training of specialists in these sectors and actively supports the energy transition and sustainable development in Senegal and the wider region.

Dr. Youssou GNING is a lecturer and researcher in the Physics Department of the Faculty of Science and Technology at Iba Der THIAM University in Thiès. Dr. GNING completed a PhD thesis in Atomic and Nuclear Physics at Cheikh Anta DIOP University in Dakar. As part of this research, Dr. GNING has published on the study of resonance parameters (resonance energies and widths) of multi-electron atomic systems using variational methods. Consequently, these methods allow for a better understanding of excitation and de-excitation processes, highlighting the importance of electronic correlation phenomena in nuclear systems, and exploring broader areas of the electromagnetic spectrum through the use of very intense light sources (synchrotron radiation sources and lasers). As part of expanding his research field, Dr. GNING also studies complex systems, materials, as well as the field of bioenergy and biogas.

Aly TOURE, and I am currently a third-year PhD student in Science and Technology at the University Iba Der Thiam of Thiès, Senegal. I hold a Bachelor's degree in Physics and Chemistry and a Master's degree in Renewable Energies. My current research focuses on renewable energy physics, with a particular emphasis on photovoltaic solar energy. I have developed strong skills in modelling and simulation of photovoltaic devices using ATLAS-Silvaco and Matlab-Simulink, as well as in the optimisation and electrical/optical characterisation of photovoltaic solar cells. My work contributes to the understanding, performance improvement, and optimization of solar technologies for sustainable development.

Ahmed Mohamed Yahya has been serving as an Associate Professor in the Department of Physics at the University of Nouakchott, Mauritania, since 2017. In 2005, he obtained his Advanced Studies Diploma in Solar Energy from Cheikh Anta Diop University in Dakar, Senegal, and in 2012, he earned his Ph.D. in Solar Energy, Materials, and Systems from the same Senegalese university. Author has contributed to scientific research as an author and co-author of over 20 technical articles

published in international journals and conferences, as well as two book chapters. He also possesses extensive experience in the field of electrical energy, especially in renewable energies. He has worked with various companies and public institutions, accumulating significant expertise in feasibility studies for projects such as photovoltaic solar power plants, wind farms, solar-powered public lighting, measurement stations, medium and low-voltage electrical networks, ice production facilities, and seawater desalination.